J Physiol 587.18 (2009) pp 4543–4559

Simultaneous recording of intramembrane charge movement components and calcium release in wild-type and S100A1$^{-/-}$ muscle fibres

Benjamin L. Prosser[1], Erick O. Hernández-Ochoa[1], Danna B. Zimmer[2] and Martin F. Schneider[1]

[1]*Department of Biochemistry and Molecular Biology, University of Maryland School of Medicine, 108 N. Greene Street, Baltimore, MD 21201, USA*
[2]*Department of Veterinary Pathobiology, College of Veterinary Medicine, Texas A&M University, College Station, TX 77843-4467, USA*

In the preceding paper, we reported that flexor digitorum brevis (FDB) muscle fibres from S100A1 knock-out (KO) mice exhibit a selective suppression of the delayed, steeply voltage-dependent component of intra-membrane charge movement current termed Q_γ. Here, we use 50 μM of the Ca^{2+} indicator fluo-4 in the whole cell patch clamp pipette, in addition to 20 mM EGTA and other constituents included for the charge movement studies, and calculate the SR Ca^{2+} release flux from the fluo-4 signals during voltage clamp depolarizations. Ca^{2+} release flux is decreased in amplitude by the same fraction at all voltages in fibres from S100A1 KO mice compared to fibres from wild-type (WT) littermates, but unchanged in time course at each pulse membrane potential. There is a strong correlation between the time course and magnitude of release flux and the development of Q_γ. The decreased Ca^{2+} release in KO fibres is likely to account for the suppression of Q_γ in these fibres. Consistent with this interpretation, 4-chloro-*m*-cresol (4-CMC; 100 μM) increases the rate of Ca^{2+} release and restores Q_γ at intermediate depolarizations in fibres from KO mice, but does not increase Ca^{2+} release or restore Q_γ at large depolarizations. Our findings are consistent with similar activation kinetics for SR Ca^{2+} channels in both WT and KO fibres, but decreased Ca^{2+} release in the KO fibres possibly due to shorter SR channel open times. The decreased Ca^{2+} release at each voltage is insufficient to activate Q_γ in fibres lacking S100A1.

(Resubmitted 22 June 2009; accepted after revision 31 July 2009; first published online 3 August 2009)
Corresponding author M. F. Schneider: 108 N. Greene Street, Baltimore, MD 21201, USA.
Email: mschneid@umaryland.edu

Abbreviations CaM, calmodulin; 4-CMC, 4-chloro-*m*-cresol; DHPR, dihydropyridine receptor; FDB, flexor digitorum brevis; RyR, ryanodine receptor; SR, sarcoplasmic reticulum.

In the preceding paper (Prosser *et al.* 2009) we examined the properties of intra-membrane charge movement currents in muscle fibres from S100A1 knock-out (KO) mice and from their wild-type (WT) littermates. We found that fibres from S100A1 KO mice exhibit a selective suppression of the delayed, steeply voltage dependent component of intra-membrane charge movement termed Q_γ. In previous studies on frog skeletal muscle fibres it has been noted that there is a close temporal relationship between the Q_γ component of charge movement and the onset of Ca^{2+} release from the SR, with Q_γ being considered to be either a cause (Reviewed in Huang, 1988) or a consequence (Csernoch *et al.* 1991; García *et al.* 1991; Pizarro *et al.* 1991; Gonzalez & Rios, 1993) of Ca^{2+} release. We therefore next sought to examine the relationship between Ca^{2+} transients and charge movement under the conditions of our studies by including 50 μM of the Ca^{2+} indicator fluo-4 in the whole cell patch clamp pipette.

Here we use fluo-4 fluorescence transients, monitored with ultra-high speed confocal imaging, to calculate Ca^{2+} release during voltage clamp depolarizations in mouse flexor digitorum brevis (FDB) skeletal muscle fibres, while simultaneously monitoring charge movement currents. We find that Ca^{2+} release is decreased in amplitude by the same factor at all voltages, but unchanged in time course at any voltage in fibres from S100A1 KO mice compared to fibres from WT littermates, and that the decreased Ca^{2+} release is likely to account for the suppression of Q_γ in the KO fibres. Additionally, pharmacologically enhancing release in KO fibres with the RyR1 agonist 4-chloro-*m*-cresol at least partially rescues Q_γ, further supporting the correlation between Ca^{2+} release and the Q_γ component of intra-membrane charge movement.

DOI: 10.1113/jphysiol.2009.177246

Methods

Ethical approval

All animals were housed in a pathogen-free area at the University of Maryland, Baltimore. The animals were killed according to authorized procedures of the Institutional Animal Care and Use Committee, University of Maryland, Baltimore, by regulated delivery of compressed CO_2 overdose followed by decapitation.

FDB fibre preparation

Fibres were prepared using enzymatic dissociation of FDB muscles of 6- to 7-week-old C57 × 129 WT and S100A1 KO mice, and were cultured as previously described (Liu *et al.* 1997). S100A1$^{-/-}$ animals and WT littermate control animals were obtained from Dr Danna Zimmer, Texas A&M University. The generation and genotyping of these animals has been previously reported (Prosser *et al.* 2007).

Solutions

Except where otherwise specifically indicated, all solutions were identical to those used in the previous paper (Prosser *et al.* 2009), with the addition of 50 μM Fluo-4 to the internal solution in the patch pipette for monitoring Ca^{2+} transients in all studies in this paper.

Electrophysiology and data analysis

Membrane current measurements and quantification of intra-membrane charge movement were performed identically as described in the companion paper.

Ca^{2+} transient fluorescence recordings

Fluorescence signals were recorded during voltage clamp depolarizations using a high speed confocal system (Zeiss LSM 5 LIVE) synchronized with the patch clamp system. Fibre culture chambers were mounted on a Zeiss Axiovert 200M inverted microscope and confocal imaging was performed in linescan x–t mode as previously described (Prosser *et al.* 2007), with images acquired at 50 μs/line for 1 s acquisition. A region of interest was taken from the centre of the fibre and the change in fluorescence (ΔF) upon depolarization was averaged from this region after subtraction of background fluorescence from a region outside of the fibre. Images were analysed and processed using OriginPro 8.0 (OriginLab Corp., Northampton, MA, USA).

Calculation of Ca^{2+} release flux

Time course of free Ca^{2+} concentration. Following the analysis previously used for calculating the time course of free Ca^{2+} concentration from fura-2 fluorescence signals under conditions when the dye is not at equilibrium with the myoplasmic free Ca^{2+} (Klein *et al.* 1988), the time course of free Ca^{2+} concentration ($[Ca](t)$), is given by (Klein *et al.* 1988, eqn (5), with rearrangements):

$$[Ca](t) = K_{Dd}\{(1/k_{offd})dF(t)/dt + F(t) - F_{min}\}/\{F_{max} - F(t)\} \quad (1)$$

where K_{Dd} is the dissociation constant for Ca^{2+} from the indicator dye (here fluo-4), k_{offd} is the off rate const for Ca^{2+} dissociation from the dye, F is the fibre fluo-4 fluorescence signal and F_{max} and F_{min} are the fluorescence at saturating and zero free Ca^{2+}, respectively. Due to the presence of 20 mM EGTA in the pipette solution with no added Ca^{2+} we assume that the resting fibre fluorescence $F_0 = F_{min}$. In this case $F = F_{min} + \Delta F$ and:

$$[Ca](t) = K_{Dd}\{(1/k_{offd})d\Delta F(t)/dt + \Delta F(t)\}/(F_{max} - \Delta F(t) - F_{min}), \quad (2)$$

which is the equation used here for calculating $[Ca](t)$. This derivative term in eqn (2) introduces significant noise into the calculation of $[Ca](t)$. Therefore, for smaller depolarizing pulses that produced negligible or slowly changing fluorescence transients, we routinely set the derivative term to zero for calculating $[Ca](t)$ to improve signal to noise. Such cases can be identified in Figs 3, 4, 5 and 8 by the reduced noise level in the records of $[Ca](t)$ and calculated Ca^{2+} release for the smaller pulses (see below).

Time course of the rate of change of [Ca-EGTA]. Under the conditions of 20 mM EGTA with no added Ca^{2+} in the pipette, EGTA is the major binding site for released Ca^{2+}. In that case $d[Ca\text{-}EGTA](t)/dt$ provides a good approximation to the rate of SR Ca^{2+} release in the fibre, and will be used in the Ca^{2+} release calculations presented here. For Ca binding to EGTA,

$$d[Ca\text{-}EGTA](t)/dt = k_{one}[Ca](t)[EGTA](t) - k_{offe}[Ca\text{-}EGTA](t), \quad (3)$$

where k_{one} and k_{offe} are on and off rate constants for Ca^{2+} binding to EGTA.

Since $[EGTA](t) = [EGTA]_{tot} - [Ca\text{-}EGTA](t)$,

$$d[Ca\text{-}EGTA](t)/dt = k_{one}[Ca](t)\{[EGTA]_{tot} - [Ca\text{-}EGTA](t)\} - k_{offe}[Ca\text{-}EGTA](t). \quad (4)$$

Equation (4) was solved numerically using $[Ca](t)$ from eqn (2) and using the Euler method to calculate the time

course of d[Ca-EGTA](t)/dt, which was used as the time course of the rate of Ca^{2+} release from the SR during the voltage clamp pulses. [EGTA] at the start of each pulse was assumed to be equal to the total [EGTA] in the pipette solution and [Ca-EGTA] was correspondingly assumed to be 0 at the start of each pulse.

The parameter values used in our calculations were $K_{Dd} = 1000$ nM (Harkins *et al.* 1993), which we confirmed *in situ* using a Ca^{2+} calibration kit (Molecular Probes), $k_{offd} = 90\ s^{-1}$ (Shirokova *et al.* 1996), $k_{one} = 15\ (\mu M\ s)^{-1}$ and $k_{offe} = 7.5\ s^{-1}$ (Royer *et al.* 2008).

Extracellular application of 4-CMC

4-Chloro-*m*-cresol (4-CMC; Aldrich, Milwaukee, WI, USA) was diluted in DMSO and added directly to the external solution, which was then gently pipetted to promote uniform dilution in the bath volume.

Statistical analysis

All statistical analysis was performed using OriginPro 8.0. All data are presented as mean values ± standard error of the mean (S.E.M.) unless otherwise noted. Normality of data sets was ensured for each statistical calculation. Significance was determined using Student's t-test and set at $P < 0.05$.

Results

Fluo-4 fluorescence transients elicited by voltage clamp pulses

Figure 1 illustrates the basic protocol used to monitor Ca^{2+} transients in these studies. An FDB fibre from a WT mouse was voltage clamped at a holding potential of −80 mV with 50 μM of fluo-4 in the patch pipette. Starting 20 min after seal formation, a series of voltage clamp depolarizations of increasing amplitude (Fig. 1*A*, top) were applied to the fibre at 30 s intervals. The high speed (50 μs per line) confocal line scan images (Fig. 1*A*) synchronized with each of the pulses show a non-detectable fluorescence signal for the pulse to −40 mV, but increasing fluorescence signals for the increasingly larger depolarizations. Thus, despite the presence of 20 mM EGTA in the patch pipette solution together with the 50 μM fluo-4, we were still able to record clearly detectable voltage-dependent fluo-4 signals in response to depolarization of the voltage clamped fibres. Note that due to the presence of 20 mM EGTA in the pipette solution and its diffusion into the fibre there is no detectable sign of fibre movement in the confocal line scan images. Figure 1*B* shows the time course of fluorescence change (ΔF) in the region of interest in the middle part of the fibre (shown in white in Fig. 1*A*, bottom) for each of the pulses. Consistent with the image display (Fig. 1*A*), the extracted ΔF records showed no detectable change at −40 mV, and then increased in amplitude as well as in rate of rise, and decreased in latency as the pulse was increased from −30 to +20 mV (Fig. 1*B*). There is no sign of fibre movement in the fluorescence change signals in Fig. 1*B*, or in any other record obtained in this study.

Basis for resting fibre fluo-4 fluorescence, and estimation of fluo-4 F_{min}

Fluorescence signals from Ca^{2+} indicator dyes depend on the concentrations of both Ca^{2+} and dye, as well as other

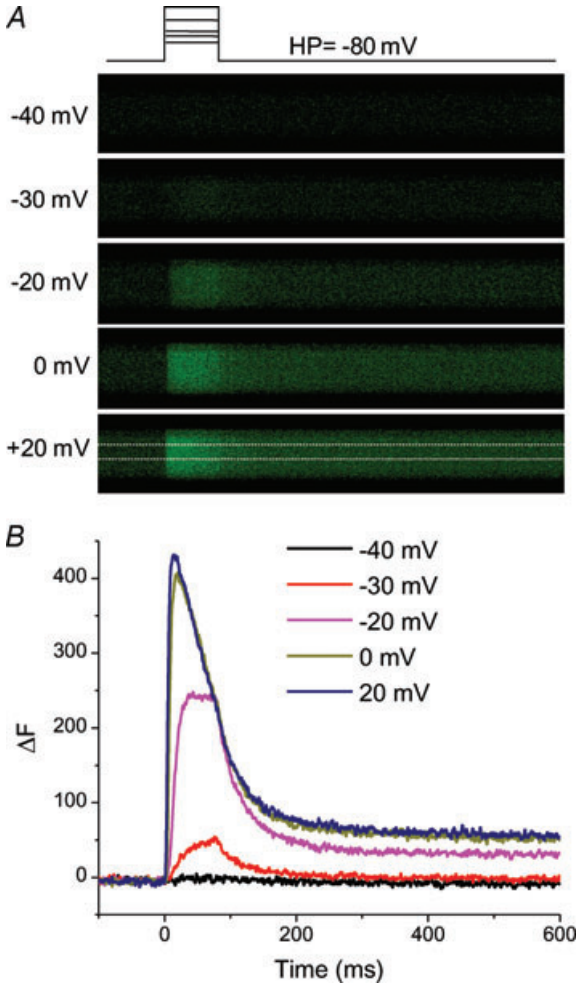

Figure 1. Fluo-4 Ca^{2+} transients elicited by step depolarizations in a control voltage-clamped FDB fibre
A, high speed (50 μs per line) confocal line scan x–t images synchronized with pulse protocol drawn above. Time scale is same as in *B*. The white box in the bottom panel (pulse to +20 mV) represents the region of interest drawn in the centre of the fibre that was averaged to calculate the change in fluorescence intensity. *B*, time course of change in fluo-4 fluorescence (ΔF) recorded from pulses above. A change in fluo-4 fluorescence was typically first detected at pulses to −30 mV, and saturated with pulses around +20 mV.

divalent cations that may interact with the dye. Since fluo-4 is not a ratiometric Ca^{2+} indicator dye, the effects of Ca^{2+} and dye concentrations cannot be separated by using ratiometric recording. However, since 20 mM EGTA was present in the patch pipette together with 50 μM fluo-4, we expected that fluo-4 would be essentially fully Ca^{2+} free in the resting fibre. In that case the fibre resting fluorescence would be expected to provide a direct measure of F_{min}, the fluo-4 fluorescence in the fibre at zero $[Ca^{2+}]$.

We next examined fibre resting fluorescence and how it changed over time, with and without application of repeated depolarizing pulses over a time interval corresponding to our standard experimental recording period. As shown diagrammatically at the bottom of Fig. 2*A*, starting exactly 20 min after the time of establishing the whole cell recording configuration, fibres were first subjected to a series of four depolarizing steps to +10 mV applied at 30 s intervals, then to four steps to −60 mV at 30 s intervals and then again to four steps to +10 mV at 30 s intervals (all pulses 80 ms in duration). In three fibres bathed in our standard external solution (containing 0.5 mM Cd^{2+} and 0.5 mM Co^{2+}) and studied with this pulse protocol, the fibre resting fluorescence prior to each pulse increased steadily over the course of the experiment (Fig. 2*A*, filled circles), both during the two sets of pulses to +10 mV (22 and 24% increase per min, respectively) and during the set of pulses to −60 mV (16% per min). As there was a significant time-dependent increase in resting fluorescence in our standard external solution even with sub-threshold stimulation that did not produce detectable fluo-4 ΔF Ca^{2+} transients (Fig. 2*A*, middle filled circles),

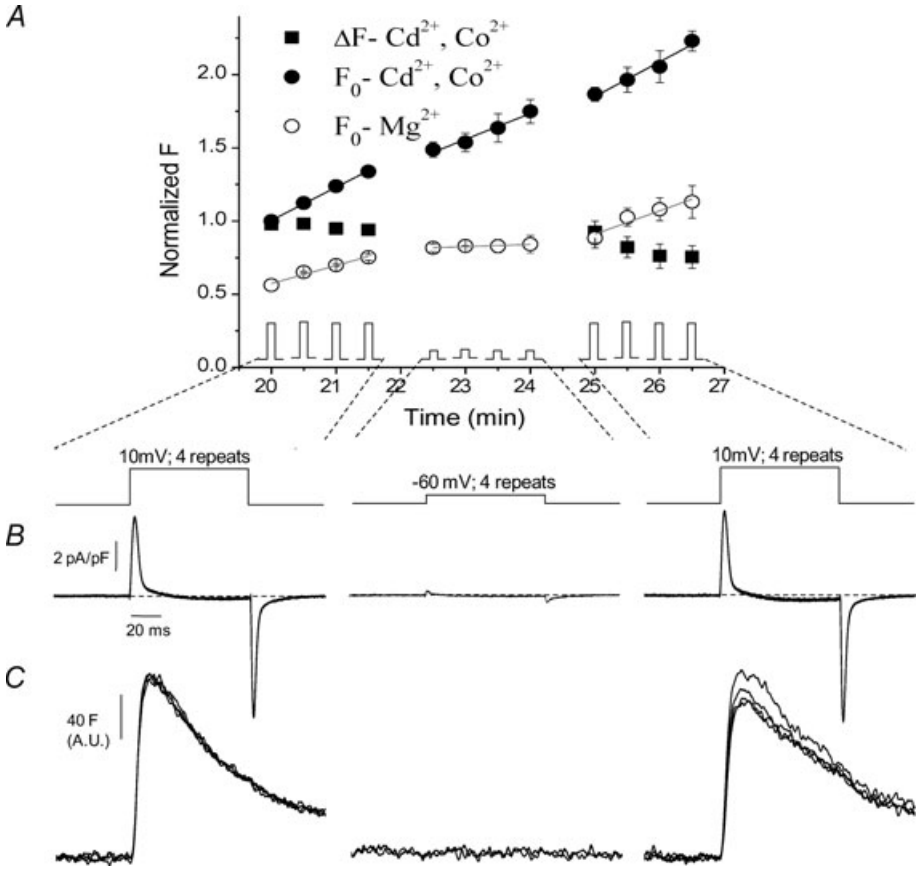

Figure 2. Evaluation of resting fluorescence, evoked fluorescence transients, and charge movement currents during repetitive pulses in fibres exposed to an external solution with or without Cd^{2+} and Co^{2+}

A, F_0 and ΔF plotted against time of dialysis with 50 μM fluo-4 in the patch pipette. The first four points represent pulses from −80 mV to +10 mV, the second four represent pulses to −60 mV, and the last four repeat pulses to +10 mV. As can be seen the resting fluorescence (F_0) steadily increases with time, even with pulses to −60 mV where there is no detectable release, in the presence (F_0-Cd^{2+}, Co^{2+}; filled circles), but not in the absence of Cd^{2+} and Co^{2+} (F_0-Mg^{2+}; open circles). The initial F_0 value in both solutions was normalized to the initial value in the Cd^{2+}/Co^{2+} containing solution to appreciate differences in F_0 at the start of the experimental protocol. *B*, charge movement records from pulses in *A* show that charge movement currents are preserved with repeated pulsing and time in solution. *C*, ΔF records from pulses in *A* (ΔF-Cd^{2+}, Co^{2+}; filled squares) show stability of ΔF recordings, despite elevation in F_0, with repetitive pulsing. Some slight rundown with time is evident after 25 min.

the increase in resting fluorescence with time during the periods of supra-threshold stimulation that did cause Ca^{2+} release was likely to be due to accumulation in the cytoplasm of previously released Ca^{2+}, as well as an additional time-dependent elevation in fluorescence independent of Ca^{2+} accumulation.

In contrast, when Cd^{2+} and Co^{2+} were eliminated from the bathing medium, the resting fluorescence only increased due to Ca^{2+} accumulation. The time-dependent increase in resting fibre fluorescence (Fig. 2*A*, open circles) was essentially eliminated during the subthreshold pulses to −60 mV (1% per min), when there was no detectable Ca^{2+} release. When there was significant Ca^{2+} release (Fig. 2*A*, open circles left and right), fluorescence increased, but at a reduced rate (12 and 18% per min, respectively) compared to fibres bathed in the Cd^{2+} and Co^{2+} containing solution. Thus, independent of changes in free Ca^{2+} concentration, the presence of Cd^{2+} and Co^{2+} seems to promote a time-dependent increase in fibre fluorescence, as has been previously documented in other cell types (Hinkle *et al.* 1992; Shibuya and Douglas, 1992; Schaefer *et al.* 1994). Consistent with this idea, 20 min after the whole cell clamp condition was established, the mean fibre fluorescence was 1.78 ± 0.09 times higher ($P < 0.05$) in fibres in the Cd^{2+} and Co^{2+} solution than in fibres in the Cd^{2+} and Co^{2+}-free external solution containing 2 mM Mg^{2+} (Fig. 2*A*, left most filled and open circles, respectively). Since there were no pulses applied during the 20 min equilibration period, we conclude that the presence of Cd^{2+} and Co^{2+} in the bathing solution artifactually raises the fibre fluo-4 fluorescence, possibly due to Cd^{2+} and/or Co^{2+} binding to fluo-4 in the fibre. A similar time-dependent increase in fibre resting fluorescence occurs in intact FDB fibres pre-loaded with fluo-4AM and subsequently exposed to Cd^{2+} or Co^{2+} in the bathing solution (Prosser *et al.* unpublished observation). Since the ratio of fluorescence of fibres in the two solutions in Fig. 2 was highly reproducible at 20 min after the whole cell configuration was established (Fig. 2*A*), we scaled the starting fluorescence recorded at 20 min in each fibre in the Cd^{2+} and Co^{2+} solution by the factor 0.56 (= 1/1.78), and used this as F_{min} for all calculations of Ca^{2+} concentration or of Ca^{2+} release for that fibre.

The increase in fibre resting fluorescence observed during the course of the experiment (Fig. 2*A*, filled circles) might be assumed to indicate an increase in fluo-4 concentration in the fibre with time. In this case, if Ca^{2+} release were constant we would then expect that there should be a parallel increase in the fluorescence signal for a given pulse. However, this was not the case. Figure 2*A* (filled squares) and Fig. 2*C*, left and right traces, show that the fluo-4 ΔF transients did not increase with time during the experiment, but were similar from pulse to pulse when the same 80 ms pulse to +10 mV was repeatedly applied 4 times at 30 s intervals either early or late during the experiment. A slight decline of ΔF, presumably due to fibre run-down, was seen during the second set of pulses to +10 mV (Fig. 2*A* filled squares, right, and Fig. 2*C*, right traces). The simultaneously recorded charge movement currents for the two groups of repeated pulses to +10 mV were also highly reproducible (Fig. 2*B*). Thus both Ca^{2+} transients and charge movement were stable in voltage clamped fibres during repeated application of the same pulse using our standard bathing and pipette solutions (plus 50 μM fluo-4 in the pipette). The constancy of the ΔF transients for repeated pulses suggests that despite the possible partial occupancy of the dye by Cd^{2+} and/or Co^{2+}, the diffusion of free dye from the pipette is sufficient to maintain a relatively constant level of free dye in the fibre.

Ca^{2+} transients and Ca^{2+} release flux in wild-type fibres

Figure 3*A* presents the fluo-4 ΔF records for the family of pulses in Fig. 1 now replotted on an expanded time scale. Figure 3*B* presents the corresponding Ca^{2+} transients calculated from the fluorescence signals in Fig. 3*A* by eqn (2), and Fig. 3*C* presents the rate of release of Ca^{2+} from the SR as calculated from the Ca^{2+} records using eqn ((4). Under the present conditions of high EGTA buffering, the Ca^{2+} release time course was quite similar to that of the free Ca^{2+}. As previously described for both frog (Melzer *et al.* 1984) and rodent (Delbono & Stefani, 1993; Royer *et al.* 2008) muscle, the Ca^{2+} release waveform for the larger depolarizing pulses exhibited a pronounced early peak followed by a subsequent rapid and then a slower decline with time, likely to be reflecting partial inactivation of the RyR Ca^{2+} release channel and decline of SR Ca^{2+} content, respectively (Schneider & Simon, 1988; Simon *et al.* 1991). For smaller pulses the relative decline in Ca^{2+} release during the pulse was much less than for the larger pulses, consistent with less cumulative inactivation of RyR Ca^{2+} release channels at the lower level of RyR channel activation during smaller depolarizations (Klein *et al.* 1997).

S100A1 KO muscle fibres have suppressed Ca^{2+} release amplitude, but exhibit Ca^{2+} release kinetics highly similar to that of WT fibres

Figure 4*A* presents the average of the Ca^{2+} release records obtained from nine WT fibres for 80 ms pulses to −40 through +20 mV in 10 mV steps, and Fig. 4*B* presents the comparable set of average release records for pulses to the same voltages in eight KO fibres. The release at each voltage is smaller in the KO than in the WT fibres, but the time courses of the two sets of records are remarkably similar, as will be considered further below. The amplitude of the average peak rate of Ca^{2+} release was considerably greater

at each voltage for the WT compared to the KO fibres (Fig. 4*C*), but the voltage dependence was very similar. As a first approximation, average voltage dependence of peak rate of release data from both the WT and the KO fibres (Fig. 4*C*) of each individual fibre tested was fitted to a single Boltzmann function, as described by the equation:

$$R(V) = R_{\max}/(1 + \exp((V_{\text{half}} - V)/k)), \qquad (5)$$

where $R_{\max}$ gives the maximum release rate, V_{half} defines the potential where $R = 0.5$ of $R_{\max}$, and $1/k$ is a measure of the steepness of the maximum release rate *versus* V relationship. The parameter values for the fit of the Boltzmann relationship to the WT data were 57 μM ms^{-1} for $R_{\max}$, 8.3 mV for the steepness factor (k) and −9.5 mV for the mid-point voltage (V_{half}), with corresponding values of 32 μM ms^{-1}, 8.4 mV and −10.9 mV for the fit to the average KO data. The average values for the parameters for fits to the voltage dependence of peak release for the individual fibres were 56 ± 8 μM ms^{-1} for $R_{\max}$, 7.9 ± 0.3 mV for k and -10.5 ± 1.7 mV for V_{half} in WT fibres and 32 ± 8 μM ms^{-1} ($P < 0.01$), 8.1 ± 0.6 mV (NS) and -9.9 ± 1.5 mV (NS) for KO fibres. Thus aside from the greater amplitude of release at all voltages, the relative voltage dependence of release was essentially identical for fibres from WT and S100A1 KO animals, as shown by the scaled up voltage dependence of release from the KO fibres which essentially superimposes on that of the WT fibres (Fig. 4*C*).

Figure 4*D* plots the voltage dependence of release determined here together with the voltage dependence of charge movement, analysed in detail in the previous paper (Prosser *et al.* 2009). KO traces were normalized to corresponding WT Q or R values to provide a comparison of the proportional suppression of release and charge. Both WT and KO fibres demonstrated significant charge movement prior to detectable release. As can be seen the Q *vs.* V relationship was virtually identical in both WT and KO fibres up to the onset of detectable release at −30 mV. The Q–V plots then began to diverge upon further depolarization, with greater charge moved in the WT fibres concomitant with their increased release flux compared to KO counterparts. Differences in both release and charge in WT *versus* KO fibres continued to increase with further depolarization, and then saturated around +10 mV. Maximal charge was suppressed by ∼30% in KO fibres, whereas maximal release was suppressed by ∼43%. These results suggest a close correlation in the voltage dependence of suppressed Ca^{2+} release and the suppressed component of intra-membrane charge movement in S100A1 KO fibres.

The remaining charge in the KO represents a good approximation to Q_β, which may be responsible for the voltage-dependent activation of Ca^{2+} release in WT and KO fibres. We examined whether the voltage dependence of charge and peak Ca^{2+} release flux exhibited a relationship similar to that described by Simon & Hill (1992) for amphibian muscle fibres by fitting the

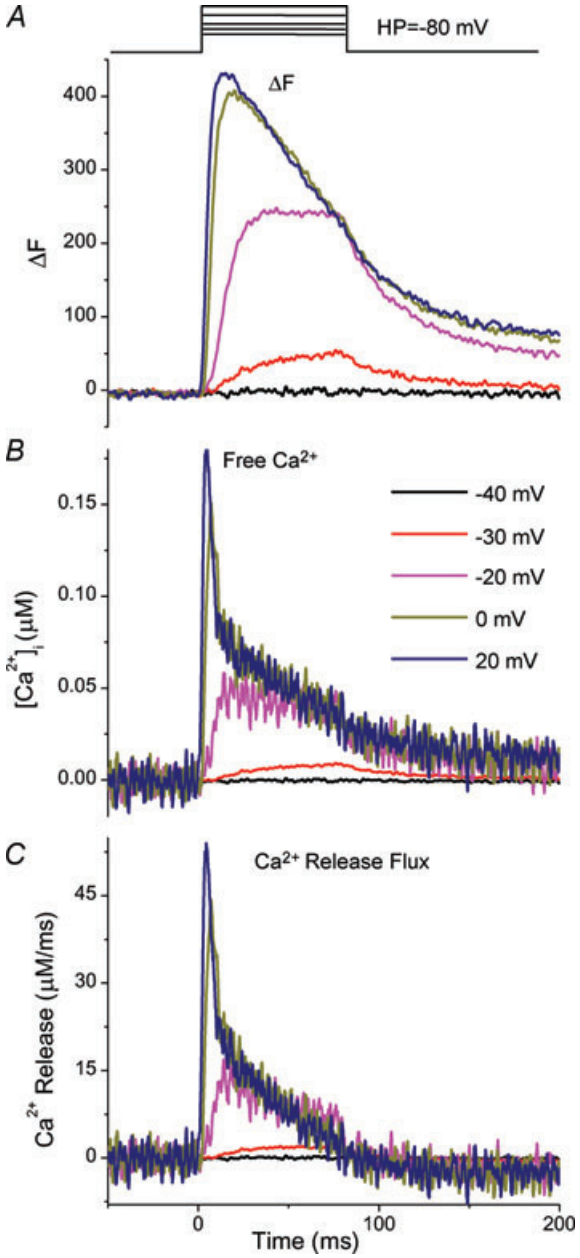

Figure 3. Calculation of voltage-dependent Ca^{2+} release flux from fluo-4 Δ*F* transients
A, experimentally measured fluo-4 Δ*F* records from Fig. 1*B*, now expanded in time, with pulse protocol above and time scale at bottom of *C*. *B*, free Ca^{2+} waveforms derived from *A* and calculated using eqn (2) (see Methods). *C*, Ca^{2+} release flux derived from *B*, calculated using eqn (4) with 20 mM EGTA in the internal solution. EGTA is the major intracellular binding site for released Ca^{2+}, and therefore the rate of Ca^{2+} binding to EGTA can be used as a first approximation of the rate of Ca^{2+} release. In *B* and *C*, for pulses to −40 and −30 mV, the derivative term from eqn (2) (see Methods) has been set to zero to improve signal to noise.

normalized KO/WT R *vs.* V relationship (essentially identical in WT and KO fibres, as depicted in Fig. 4*C*) to the KO Q *vs.* V relationship (representing Q_β) elevated to the fourth power. $Q_\beta{}^4(V)$ did not accurately describe the $R(V)$ relationship, as it was right shifted along the voltage axis and slightly less steep than the $R(V)$ fit, exhibiting a V_{half} of −4.6 mV and a k value of 9.2 mV (compared to −10 mV and 8 mV for the V_{half} and k of $R(V)$, respectively). The reason for this discrepancy is unknown, although it may stem from the fact that Simon & Hill utilized a different stimulation protocol to isolate the non-inactivatable component of Ca^{2+} release, whereas here we evaluated the peak release flux with variable inactivation inherent in our recordings.

The average rate of Ca^{2+} release records from Fig. 4 are re-plotted in Fig. 5 on an expanded time scale, but with the average Ca^{2+} release records from the KO fibres now scaled up to match the peak amplitude of the average WT records at the same pulse voltage. This comparison of the scaled records indicates that the relative time course of the release records for WT and KO fibres were virtually identical at all voltages examined. Temporal expansion of the initial phase of the Ca^{2+} release records (inset for 0 and +20 mV records) indicates that the latency and the time to peak of the normalized records were also essentially indistinguishable in the WT and KO fibres. This remarkable constancy of relative time course, but different amplitudes, of the average Ca^{2+} release records in the KO compared to the WT fibres, as well as the identical voltage dependence but smaller amplitude in the KO compared to the WT fibres, is consistent with an identical opening pattern for both the WT and KO RyR Ca^{2+} release channels, but with longer mean channel open time in the presence (WT) compared to the absence (KO) of S100A1, as previously reported for RyR1 Ca^{2+} channels in lipid bilayer membranes (Treves *et al.* 1997).

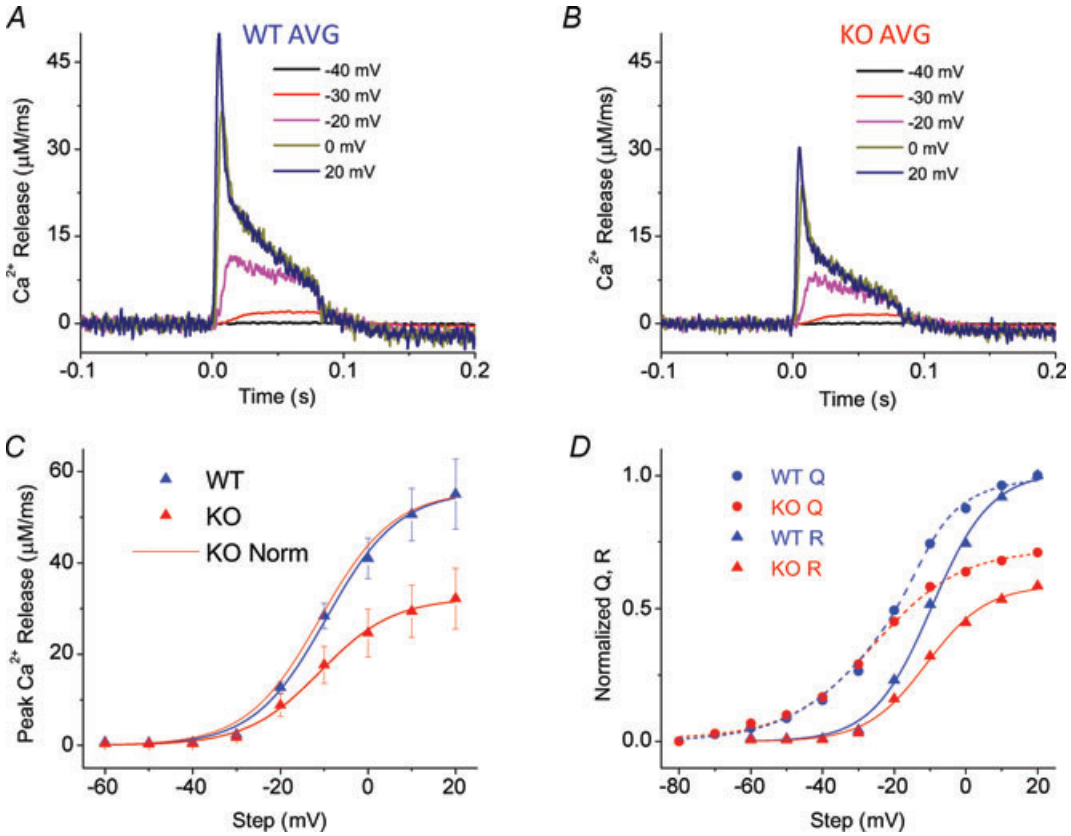

Figure 4. Peak rate of Ca^{2+} release is decreased at all voltages in S100A1 KO fibres
A, average records of Ca^{2+} release flux from WT fibres ($n = 9$). *B*, average records of flux from KO fibres ($n = 8$), plotted on same scale as *A* to appreciate differences in release amplitude. *C*, peak release (R) plotted *vs.* voltage. Continuous lines through the symbols are best fits to a single Boltzmann function (eqn (5)) with parameters of 57 μM ms^{-1} for R_{max}, 8.3 mV for k and −9.5 mV for V_{half} for average WT data, with corresponding values of 32 μM ms^{-1}, 8.4 mV and −10.9 mV for the average KO fibres. The continuous red trace represents the fit to the KO average scaled up to the WT maximum to show virtually identical voltage dependence between WT and KO fibres. *D*, WT and KO R plotted *vs.* WT and KO charge movement from companion paper (Prosser *et al.* 2009). Traces are normalized to WT maximum R and Q to appreciate proportional differences.

Ca^{2+} release amplitude is strongly correlated to the presence of Q_γ in both WT and KO fibres

As considered in the preceding paper (Prosser *et al.* 2009 paper), there is a range of charge movement phenotypes within both the WT and the KO fibres, with a small fraction of atypical WT fibres exhibiting little or no Q_γ component of charge movement (Fig. 6*A* and *B*, left, WT orange records) and a small fraction of atypical KO fibres exhibiting definite Q_γ (Fig. 6*A* and *B*, left, KO green records). In the fibres studied here, two of the 11 WT fibres lacked Q_γ. Two exhibited slight Q_γ and seven had definite Q_γ, whereas for the 11 KO fibres seven lacked Q_γ, two had slight Q_γ and two had definite Q_γ. Figure 6*A* (left) shows charge movement ON records from a step to −10 mV, where Q_γ is typically most prominent, in representative WT and KO fibres to demonstrate these three classifications. Figure 6*B* shows charge movement records in these same fibres from a step to +20 mV, where the difference in charge is still evident but there is no distinguishable 'hump' component. To the right of these charge records are the corresponding Ca^{2+} release records. Within both the WT and the KO fibre populations, there was a clear correlation in which fibres with definite Q_γ had larger peak Ca^{2+} release, and fibres without Q_γ had lower Ca^{2+} release (Fig. 6*C*, and individual unscaled Ca^{2+} release records in Fig. 6*A* and *B*). Within each group (WT and KO), the normalized release time courses were again similar for the fibres exhibiting low or high Q_γ, and correspondingly low or high release (Fig. 6*B*, right). These findings suggest a clear correlation between the amplitude of Ca^{2+} release flux, independent of release kinetics, and the presence (or absence) of Q_γ in both WT and KO fibres.

Comparisons of charge movement and Ca^{2+} release time course in fibres exhibiting or lacking Q_γ

For best examination of the temporal relationship between Ca^{2+} release and charge movement currents in fibres with or without Q_γ, we averaged the release records and charge movement current records for only the seven WT fibres in Fig. 6 exhibiting definite Q_γ and for only the seven KO fibres in Fig. 6 lacking Q_γ. Figure 7 presents the resulting sets of records, as well as the Q_γ current record (green), calculated at each voltage as the difference in the charge movement currents, for pulses to four different voltages. At each voltage, the Q_γ component developed at a time roughly corresponding to the start of the rising phase of the Ca^{2+} transient (Fig. 7, first vertical dashed line at each voltage) and, particularly at more positive depolarizations, peaked at a time corresponding to the time of peak of the Ca^{2+} release records (second vertical dashed line at each voltage). The decreasing time window between the two dashed lines with increasing voltage denotes the diminishing time window between the latency and the peak rate of Ca^{2+} release with increasing depolarization. Note additionally that this time window, and correspondingly the time of initial rise and peak of the Ca^{2+} release records, was virtually identical between groups at each voltage. In contrast, the peak of the charge movement currents was clearly delayed in WT fibres demonstrating Q_γ, presumably as it developed in close conjunction with the relatively greater release in WT *vs.* KO fibres. Despite the relatively large, delayed additional charge moved in these WT fibres demonstrating definite Q_γ compared to KO fibres with no Q_γ, there were no readily detectable differences in either the relative time

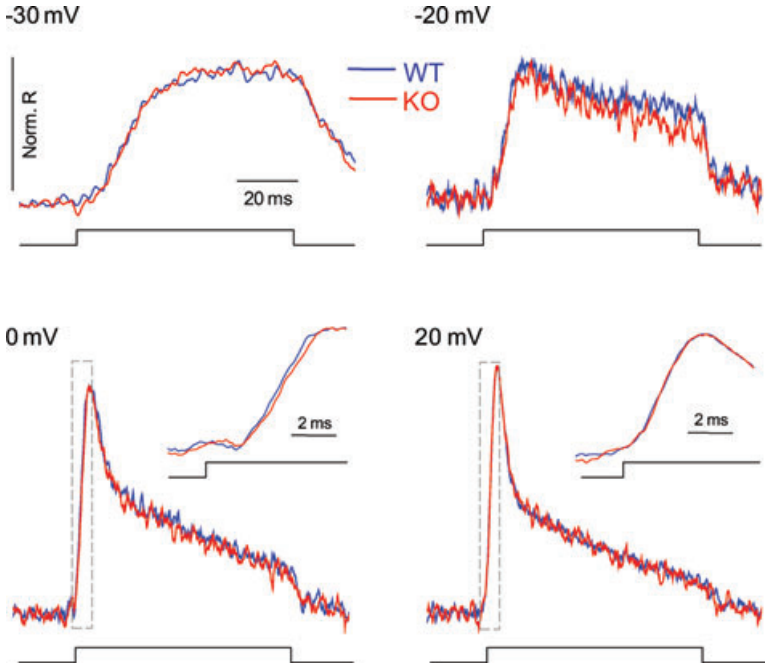

Figure 5. WT (blue trace) and KO (red trace) fibres demonstrate virtually identical relative time courses of Ca^{2+} release
Average Ca^{2+} release time courses from designated voltage steps in WT and KO fibres. Inset in bottom two panels shows zoom in of the rising phase of the rate of Ca^{2+} release peak, demonstrating virtually identical time course of release.

course of release flux or voltage dependence of release between these groups at any voltage tested (see online Supplemental Fig. 1), similar to the result found for the pooled data of all WT and KO fibres in Figs 4 and 5. These temporal relationships were as expected if Ca^{2+} release were causing the Q_γ component.

4-CMC potentiates Ca^{2+} release and Q_γ in a voltage-dependent manner in S100A1 KO fibres

Our present results clearly demonstrate that suppression of Ca^{2+} release in fibres from S100A1 KO mice compared to WT littermates, without any alteration in voltage dependence or relative time course, is correlated with a suppression of Q_γ. However, in a few atypical KO fibres demonstrating release similar to that of WT counterparts, Q_γ could be detected. Therefore if Q_γ were caused by the typically increased amplitude of release in WT compared to KO fibres, pharmacological potentiation of Ca^{2+} release in KO fibres should restore the missing Q_γ. 4-CMC is a potent and specific agonist of RyR1 Ca^{2+} release (Zorzato *et al.* 1993; Herrmann-Frank *et al.* 1996; Westerblad *et al.* 1998). High concentrations of 4-CMC ($\sim$1 mM) trigger a large release of SR Ca^{2+} in mammalian fibres without any electrical stimulation (Jiménez-Moreno *et al.* 2008). However, Westerblad *et al.* (1998) showed that at lower concentrations (100 μM) 4-CMC leads to a potentiation of released Ca^{2+} upon tetanic stimulation of FDB fibres, importantly without triggering significant resting release, as these authors showed less than a 10 nM change in resting Ca^{2+} after 10 min of 100 μM 4-CMC. In preliminary experiments, we confirmed that a 60 s exposure to 100 μM 4-CMC does in fact lead to a large potentiation of Ca^{2+} release in electrically stimulated KO fibres, without any significant change in the resting fibre fluorescence ($2.4 \pm 2.1\%$ increase in F_0 with 4-CMC, $P > 0.8$). Therefore, we designed the following experiment

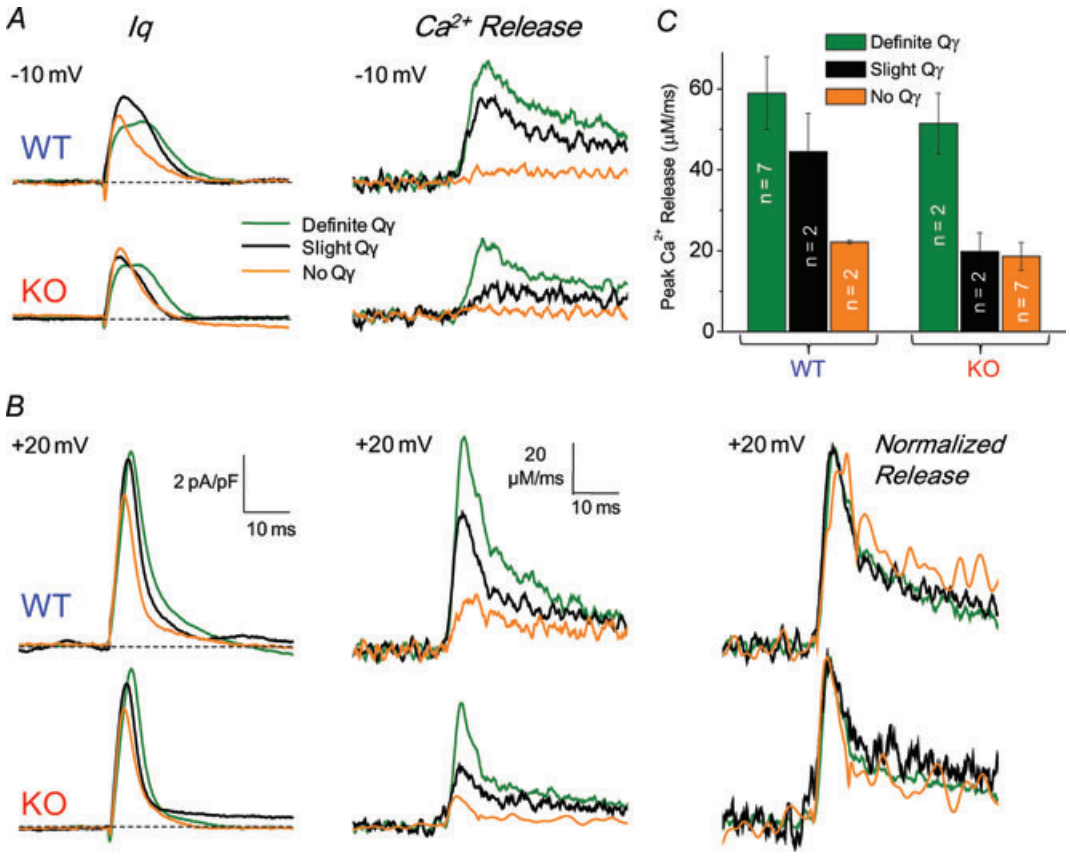

Figure 6. Correlation between Q_γ and Ca^{2+} release in WT and KO fibres
A and *B*, charge movement currents (left column traces) elicited by steps to −10 mV (top) and +20 mV (bottom) in representative WT and KO fibres demonstrating definite (green traces), slight (black traces), and no Q_γ (orange traces). Ca^{2+} release records (middle column traces) from these same fibres at each voltage. Note the correlation between the presence or absence of Q_γ and the peak of Ca^{2+} release. Right-most traces in *B* show normalized release records from +20 mV steps, showing that despite variable presence/absence of Q_γ, the relative time course of Ca^{2+} release is virtually identical in WT and KO fibres. *C*, bar plot showing distribution of WT and KO fibres demonstrating definite, slight and no Q_γ, and average peak release in these groups.

to test the effect of 4-CMC potentiation on RyR1 Ca^{2+} release and charge movement in KO fibres. Twenty minutes after establishing whole cell voltage clamp in the control extracellular solution, fibres from KO mice were first characterized for Ca^{2+} release and charge movement using the standard family of depolarizing pulses. Then, starting 60 s after adding 100 μM 4-CMC to the bathing solution, the same family of pulses was repeated on each fibre. In the presence of 4-CMC, Ca^{2+} release was detected at smaller depolarizations in all six KO fibres tested, and was considerably larger at intermediate depolarizations than in its absence (Fig. 8*A*). At the largest depolarizations the Ca^{2+} release records were very similar in the presence and absence of 4-CMC (Fig. 8*A*). The net result was thus a leftward shift in the voltage dependence of the peak rate of Ca^{2+} release after addition of 4-CMC (Fig. 8*B*). This leftward shift seen in mammalian fibres differs from the effects of 4-CMC seen in amphibian fibres, where release was increased without a leftward shift in the half-maximal voltage (Struk & Melzer, 1999).

The parameter values for the fit of the Boltzmann relationship to the average data from these six KO fibres were 31.1 μM ms^{-1} for the maximum release rate (R_{max}), 9.5 mV for the steepness factor (k) and −9.9 mV for the mid-point voltage (V_{half}), with corresponding values of 33.5 μM ms^{-1}, 9.5 mV and −21.1 mV for the fit to the average data for KO fibres treated with 4-CMC (Fig. 8*B*, curves). The average values of the Boltzmann parameters for fits to the voltage dependence of peak release for individual KO fibres before 4-CMC treatment were 31.2 ± 4.2 μM ms^{-1} for R_{max}, 9.3 ± 0.4 mV for k and −10.0 ± 1.6 mV for V_{half}, and 33.4 ± 5.0 μM ms^{-1} (NS), 8.2 ± 0.7 mV (NS) and −21.9 ± 2.2 mV ($P < 0.01$) for KO fibres treated with 100 μM 4-CMC. Thus, 100 μM 4-CMC shifted the mid-point voltage of the voltage dependence of peak Ca^{2+} release without causing any significant change in the maximum amplitude of release or in the steepness of the voltage dependence. The difference in the voltage dependence of peak rate of Ca^{2+} release in S100A1 KO fibres in the presence compared to the absence of 4-CMC thus exhibited a peak at intermediate depolarizations (Fig. 8*B* and *C*). This is in clear contrast to the difference in the voltage dependence of Ca^{2+} release between KO and WT fibres, where the maximal release was different, with no difference in midpoint voltage or steepness, so that the difference curve of WT – KO fibres had the same voltage dependence as the release in either KO or WT fibres (Fig. 8*C*, dashed curve).

Figure 9*A* presents the average charge movement currents for the same KO fibres as in Fig. 8 before and after addition of 4-CMC. At intermediate depolarizations, potentiation of release with 4-CMC elicited a temporally delayed charge movement component, similar in kinetics to the Q_γ component that is suppressed in KO compared to WT fibres. Similar to the voltage dependence of the augmentation of Ca^{2+} release by 4-CMC, the charge moved was increased at intermediate depolarizations by the presence of 4-CMC, but was much less influenced by 4-CMC at the smaller or larger depolarizations, causing the difference in charge moved (KO with minus KO without 4-CMC) to exhibit a maximum at about −20 mV (Fig. 9*A*, *B* and *C*; dark grey continuous curve). This was in sharp contrast to the difference in charge moved in WT *vs.* KO fibres, where a steep change in charge occurred

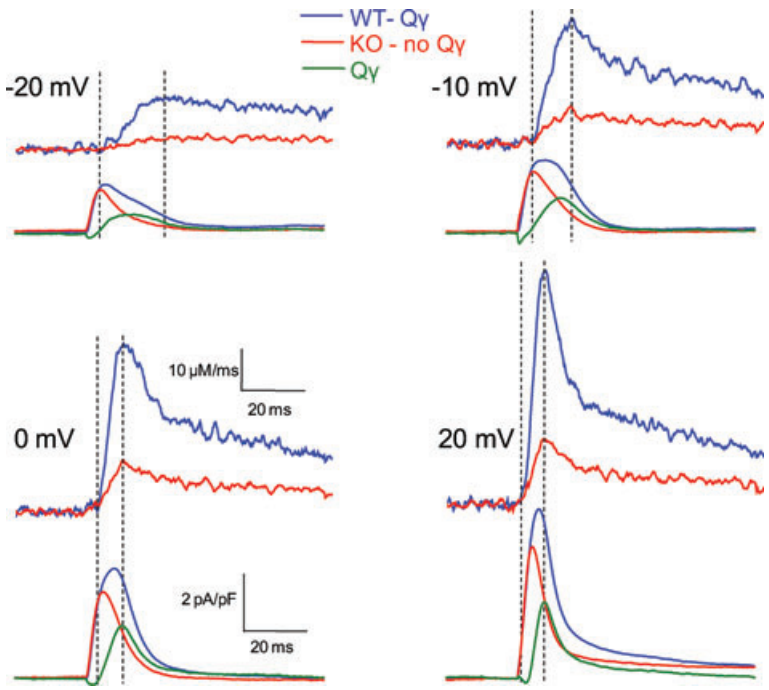

Figure 7. Temporal comparison of charge movement and Ca^{2+} release in fibres exhibiting (WT fibres, $n = 7$) or lacking (KO fibres, $n = 7$) Q_γ
Average Ca^{2+} release flux (top records each panel) and charge movement currents (bottom record each panel) are plotted in time during depolarizing steps to designated voltages. The green curve represents the difference charge current, or Q_γ current. The initial dashed line represents the start of the rising phase of Ca^{2+} release, and the following dashed line represents the peak of release. Note the development of the Q_γ current in time with release, and the similar peaks of release and the Q_γ current.

at intermediate voltages (albeit right shifted voltages) but was maintained for all further depolarizations (Fig. 9*C*, green curve). However, the steep voltage dependence of onset and current kinetics of the component elicited by the addition of 4-CMC closely resembled the Q_γ component calculated as the difference in charge movement between WT and KO fibres.

Discussion

The functional interaction between DHPR voltage sensor charge movement and RyR mediated SR Ca^{2+} release serves as the fundamental trigger of skeletal muscle EC coupling, and ultimately force generation. Here, we demonstrate for the first time in mammalian muscle fibres two clearly and reproducibly observed components of intra-membrane charge movement, monitored simultaneously with high temporal resolution characterization of SR Ca^{2+} release. We show a clear correlation between Ca^{2+} release and the Q_γ component of charge movement, and provide evidence that the Q_γ component is a consequence of release. Furthermore, we demonstrate decreased amplitude of the rate of Ca^{2+} release in fibres lacking S100A1, but an essentially identical relative time course and voltage dependence of release, when compared to WT fibres. We propose that this depressed release is the underlying cause for the suppression of Q_γ in KO fibres (Prosser *et al.* 2009). This hypothesis is strengthened by the finding that potentiating Ca^{2+} release with 4-CMC partially restores Q_γ in KO fibres.

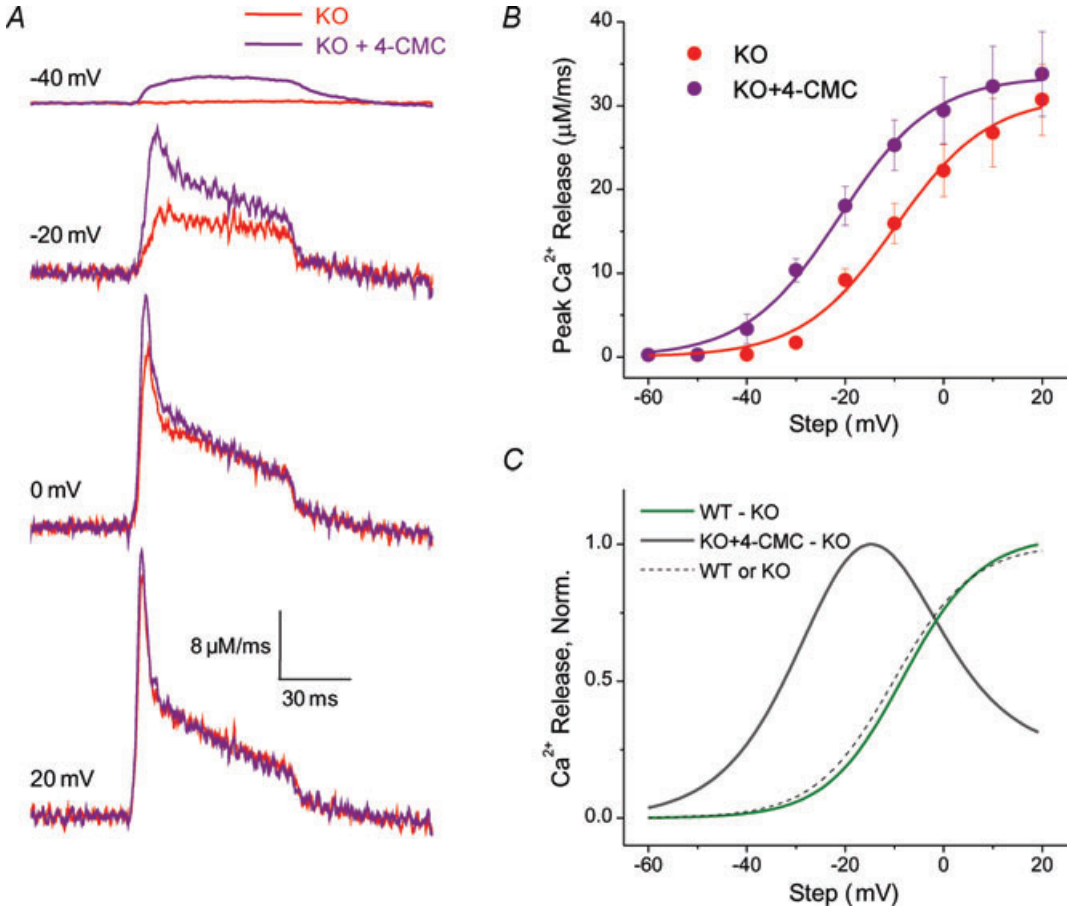

Figure 8. Potentiation of Ca^{2+} release in KO fibres by 4-CMC
A, average Ca^{2+} release records of KO fibres ($n = 6$) before (red traces) and after addition of 100 μM 4-CMC (purple traces). There was a large potentiation of release at intermediate depolarizations that diminished with increasing depolarization. *B*, *R vs. V* plot of KO fibres before (red symbols) and after application of 4-CMC (purple symbols) demonstrates a leftward shift in the voltage dependence of release imparted by 4-CMC. *C*, normalized *R vs. V* comparing the differences in Ca^{2+} release isolated from 4-CMC application to KO fibres (KO+4-CMC – KO; dark grey line) with the difference in release between WT and KO fibres (WT – KO; green line). The release augmented by 4-CMC demonstrates a leftward shift, a peak, and then diminishes with increasing depolarization, while the difference between WT and KO fibres is sustained at maximal depolarizations and exhibits a similar voltage dependence to both the WT or KO release curves (dashed line).

Q_γ: cause *vs.* consequence of SR Ca^{2+} release

Based on studies conducted primarily in amphibian muscle fibres, Q_γ has been argued to be a consequence (and perhaps an additional cause) of Ca^{2+} release from the SR. This was demonstrated by interfering with Ca^{2+} release through various methods, such as voltage-dependent inactivation of RyR1, depletion of SR Ca^{2+} stores, or pharmacological inhibition of RyR1, and monitoring the resulting effects on the hump component of charge movement currents in amphibian fibres (Csernoch *et al.* 1991; García *et al.* 1991; Pizarro *et al.* 1991; Gonzalez & Rios, 1993). These authors proposed that released Ca^{2+} ions act as a local positive feedback signal at the t-tubule membrane, driving further charge movement and possibly greater release. Therefore, interventions that suppress release also suppress a temporally delayed component of intra-membrane charge movement.

Our results in mammalian fibres generally support this model, as evidenced by the following. (1) S100A1 KO fibres demonstrate decreased peak Ca^{2+} release, but a remarkably similar time course and voltage dependence of release (Figs 4 and 5) compared to WT fibres. As Q_γ is a steeply voltage dependent and temporally delayed component of charge movement, if Q_γ were driving release we would expect to see alterations in the time course and voltage dependence of release in KO fibres that lack Q_γ. In contrast, if the depressed amplitude of release in KO fibres is altering charge movement, we would expect to see differences in charge movement current kinetics and total charge moved only at voltages where there is substantial release, as is demonstrated in Figs 4*D* and 7. It should be noted that despite the very similar relative time course of release detected here, we cannot rule out the possibility that limitations in clamp speed or

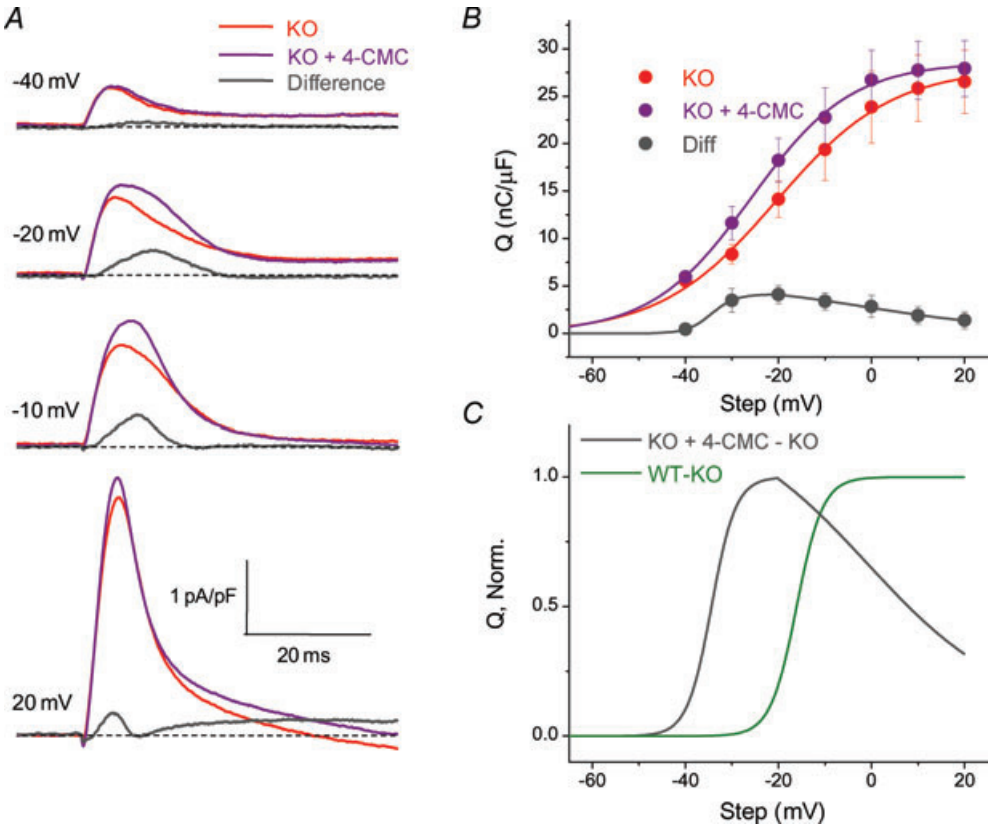

Figure 9. Potentiation of Ca^{2+} release with 4-CMC elicits a temporally delayed charge movement component in KO fibres

A, average charge movement currents in same KO fibres from Fig. 8 before (red trace) and after (purple trace) the addition of 4-CMC, with resulting difference record (KO+4-CMC – KO, dark grey trace). The addition of 4-CMC to KO fibres isolated a temporally delayed 'hump' component similar to that seen in WT fibres. *B*, *Q vs. V* relationship of KO fibres before (red symbols) and after application of 4-CMC (purple symbols), and the resulting difference charge (dark grey symbols). 4-CMC led to additional charge moved at intermediate depolarizations that diminished in magnitude with increasing depolarization in KO fibres. *C*, normalized *Q vs. V* of difference charge isolated by application of 4-CMC to KO fibres (dark grey line) compared to difference charge between WT and KO fibres (green line). Similar to release, the charge augmented by 4-CMC in KO fibres exhibits a left-shifted activation, a peak, and then declines monotonically with increasing depolarization, in contrast to the sustained additional charge isolated between WT and KO fibres.

signal to noise may prevent the detection of very subtle changes in release time course between WT and KO fibres. (2) As illustrated in Fig. 7, there is considerable charge development prior to the rise of detectable release, and Q_γ begins to develop in time with release. Additionally, there is a close temporal correlation between the peak of Ca^{2+} release and the peak of Q_γ difference current. If Q_γ were driving further Ca^{2+} release, KO fibres that lack Q_γ may be expected to demonstrate an earlier release peak than WT fibres that show Q_γ. Instead, KO and WT fibres show an essentially simultaneous peak of release, suggesting that the increased amplitude of Ca^{2+} release in WT fibres is driving this temporally delayed charge component. (3) Interventions that specifically target RyR1 mediated Ca^{2+} release and bypass the voltage sensor alter Q_γ, supporting the concept of Q_γ as a consequence of release. Specifically, potentiating release at intermediate voltages with 4-CMC restores a temporally delayed component of charge movement in KO fibres. As demonstrated in the accompanying paper (Prosser *et al.* 2009), the application of dantrolene, an RyR1 inhibitor, to WT fibres suppresses a similar temporally delayed component of charge movement current. Furthermore, S100A1 KO fibres exhibit depressed Ca^{2+} release, detailed here in voltage clamp studies, but originally S100A1 was shown to directly affect ligand activated RyR1-mediated Ca^{2+} release, in the absence of voltage sensor activation (Fano *et al.* 1989; Treves *et al.* 1997; Most *et al.* 2003). Therefore it seems likely that enhancement of release in the presence of S100A1 is driving the additional charge component seen in WT, but not in S100A1 KO, muscle fibres. Our findings in general, therefore, support the concept of local Ca^{2+} release driving additional intra-membrane charge movement, or, simply re-phrased, Q_γ being a consequence of SR Ca^{2+} release.

However, there is a notable dissimilarity between the difference component isolated by pharmacological manipulations of release, specifically application of 4-CMC to KO fibres or application of dantrolene to WT fibres, and the difference component isolated between WT and KO fibres. 4-CMC produced a leftward shift in the voltage dependence of release, augmenting release and 'rescuing' Q_γ in KO fibres only at intermediate depolarizations. This suggests that 4-CMC sensitized the RyR Ca^{2+} release channels to activation by the T-tubule voltage sensor, and thereby potentiated release to a sufficient extent at these intermediate voltages to surpass the threshold of release required to drive Q_γ. However, at maximal depolarizations (+20 mV), there was no significant enhancement of release by 4-CMC, and subsequently no additional charge moved, in these treated KO fibres. In contrast, WT fibres exhibited greater release than KO fibres at every voltage, and correspondingly moved additional charge at every voltage (Figs 8 and 9*C*). This suggests two different and possibly independent mechanisms for the enhancement of release by 4-CMC and S100A1. 4-CMC appears to increase the sensitivity of the RyR Ca^{2+} release channels to activation. Consequently, 4-CMC improves the efficiency of coupling between the voltage sensor Q_β component and release channel activation at sub-maximal activation in KO fibres, without altering the effectiveness of the Q_β component of charge movement at maximal depolarizations, where presumably all available RyRs are already activated in the absence of 4-CMC (Fig. 9*A*). S100A1, on the other hand, appears to augment release without affecting the coupling efficiency of the release channels to Q_β. One possible mechanism could be that S100A1 increases the amount of Ca^{2+} released by an active RyR channel, with no change in activation kinetics, by increasing channel open time (or increasing single channel Ca^{2+} current), so that global Ca^{2+} release is simply scaled up without changing kinetics in WT compared to S100A1 KO fibres. Additionally, we cannot rule out the possibility that S100A1 may have a secondary effect on the voltage sensor, besides simply potentiating RyR1 Ca^{2+} release, which could further alter charge movement. However, the fact that atypical S100A1 KO fibres, which demonstrate 'WT' rates of Ca^{2+} release, exhibit definite Q_γ and a similar voltage dependence of charge movement, argues against this possibility.

Mechanisms for generation of Q_γ and comparison with previous models

The fact that the total charge moved at large depolarizations in S100A1 containing fibres that exhibit greater Ca^{2+} release compared to KO fibres indicates that the extra release allows movement of a separate component of intra-membrane charge that is not moved in the S100A1 KO fibres. In contrast, adding 4-CMC to KO fibres causes an increase in charge movement at intermediate, but not at large, depolarizations. Thus, this extra charge movement at intermediate voltages could be generated by the same charged groups that move at larger depolarizations in KO fibres, but now moving at intermediate depolarizations in the presence of 4-CMC. This mechanism is similar to that proposed previously for Q_γ in amphibian fibres (Csernoch *et al.* 1991; García *et al.* 1991; Pizarro *et al.* 1991; Gonzalez & Rios, 1993). However, our finding that the total charge moved at large depolarizations is greater in WT than KO fibres is not consistent with the model for generating Q_γ by a shift in the voltage range of movement of a single group of charges. Instead, our results suggest that, in WT fibres, Q_γ may arise from a separate set of voltage sensors. The function of this charge movement component remains to be determined.

Our results with 4-CMC potentiation of Ca^{2+} release in S100A1 KO fibres raise interesting questions about the

requirements for the development of Q_γ. In KO fibres, increasing release by treatment with 4-CMC leads to the generation of Q_γ (Figs 8 and 9), but a similar increase in release produced by further depolarization of KO fibres in the absence of 4-CMC does not. If Q_γ were purely a consequence of the overall rate of release, we might expect that the Q_γ charge would just be right shifted along the voltage axis in KO compared to WT fibres, a prediction not supported by our results. This suggests that an additional factor, other than simply a necessary overall rate of release, is required for the generation of Q_γ. This additional factor could be the release per activated channel, rather than the overall release from all activated channels, implying a possible regulation of Q_γ by the local Ca^{2+} in close proximity of the activated RyR channels. However, in that case 4-CMC would have to increase the Ca^{2+} release per activated channel at the intermediate voltage range, but not increase single channel Ca^{2+} release at the larger depolarizations, in addition to sensitizing the RyR channel to activation by the DHPR. Another possibility, to be tested in future studies, is whether the peak rate of release must be sufficient to match the state or conformation of the voltage sensor in order to produce Q_γ. In this scenario, the altered state of the voltage sensor with further depolarization (perhaps the increasing kinetics of charge movement with increasing voltage) continuously raises the threshold for the peak rate of release required to trigger Q_γ. KO fibres with low rates of release simply never are able to catch up to this threshold.

Ca^{2+} transients and calculated rate of Ca^{2+} release: comparison with previous reports

In our studies we utilized an internal solution in the whole cell patch pipette containing 20 mM EGTA with no added Ca^{2+}, which should have resulted in near zero free Ca^{2+} in the resting muscle fibres 20 min after establishing the whole cell recording configuration, when our voltage clamp data acquisition began. The high intra-fibre [EGTA] also buffers the released Ca^{2+} at a very low level. Under these conditions, we used fluo-4 (50 μM) in the pipette to record the fluorescence signals during voltage clamp depolarizations, calculated the Ca^{2+} transient from the ΔF signal assuming resting Ca^{2+} prior to each pulse to be zero, and then calculated the rate of Ca^{2+} release to equal the time course of the rate of change of [Ca-EGTA]. The Ca^{2+} release waveforms recorded under these conditions generally resembled release records calculated previously, exhibiting a rapid rise to peak, followed first by a rapid decline attributed to Ca^{2+} dependent inactivation of the RyR Ca^{2+} release channel, and then a slower decline (Melzer *et al.* 1984; Delbono & Stefani, 1993). However, the slower decline seen here was considerably more rapid than recently reported by another laboratory, also using high EGTA in voltage clamped mouse FDB fibres, but with resting Ca^{2+} buffered at about 0.1 μM (Royer *et al.* 2008). The ΔF records in that paper were generally maintained during a 100 ms depolarization, whereas here the ΔF signals clearly declined during the larger 80 ms depolarizing pulses, which in turn was reflected by the relatively rapid rate of the slow phase of decline of Ca^{2+} release flux during our pulses. The source of this faster decline in release during the latter part of the pulses here is not known, but might be due to partial depletion of the SR at the very low level of cytoplasmic Ca^{2+} prior to the pulses, or possibly to some unidentified secondary effect of low resting Ca^{2+} concentration.

An interesting observation from our fluorescence records was the consistent elevation of baseline fluorescence in the presence, but not absence, of Cd^{2+} and Co^{2+} (Fig. 2*A*). These divalent cations have been previously demonstrated to interact with fluorescent Ca^{2+} indicators and produce an artificial elevation in dye fluorescence in multiple cell types other than muscle (Hinkle *et al.* 1992; Shibuya & Douglas, 1992; Schaefer *et al.* 1994). Presumably there is some permeation of these ions into the cell through cationic channels, allowing the interaction with cytosolic indicator dyes. This is of specific importance to the field of excitation–contraction coupling, as these cations are commonly used for the blocking of L-type Ca^{2+} currents, often in conjunction with fluorescence recordings. While we consistently see this artificial elevation of fluorescence in mammalian fibres, it is unclear whether this permeation into the cell occurs in amphibian fibres. We have evaluated the effects of both Cd^{2+} and Co^{2+} separately on resting fluorescence in unstimulated fibres loaded with fluo-4-AM and found a similar elevation in fluorescence, apparently independent from a rise in resting Ca^{2+} concentration, for both divalent cations.

Voltage dependence of charge movement and Ca^{2+} release

Previous studies on amphibian ileofibularis muscle fibres found a voltage dependence of Q_γ with a mid point voltage about 20 mV more negative (Pizarro *et al.* 1991; Hui, 1983) than the value of −17 mV found here in WT mouse FDB fibres. This difference in voltage dependence of Q_γ may be attributed to the right shifted voltage range found here for the appearance of Ca^{2+} release compared to the voltage range of release in frog fibres reported in some (Ríos & Pizarro, 1991; Simon & Hill, 1992) but not all (Melzer *et al.* 1986) studies on frog fibres. A similar voltage range for Ca^{2+} release as reported here in mouse FDB fibres has been previously described in rodent muscle fibres (Delbono & Stefani, 1993). In another report using mouse FDB fibres, both Ca^{2+} release and

charge movement are shifted to more positive voltages than seen here (Wang *et al.* 1999), possibly due to the presence of La^{3+} in the bathing solution, which we find leads to a positive shift in the voltage dependence of charge movement.

Model for the relationship between Ca^{2+} release and Q_γ

The results presented here clearly demonstrate that although the amplitude of the rate of Ca^{2+} release was clearly depressed at all voltages in S100A1 KO

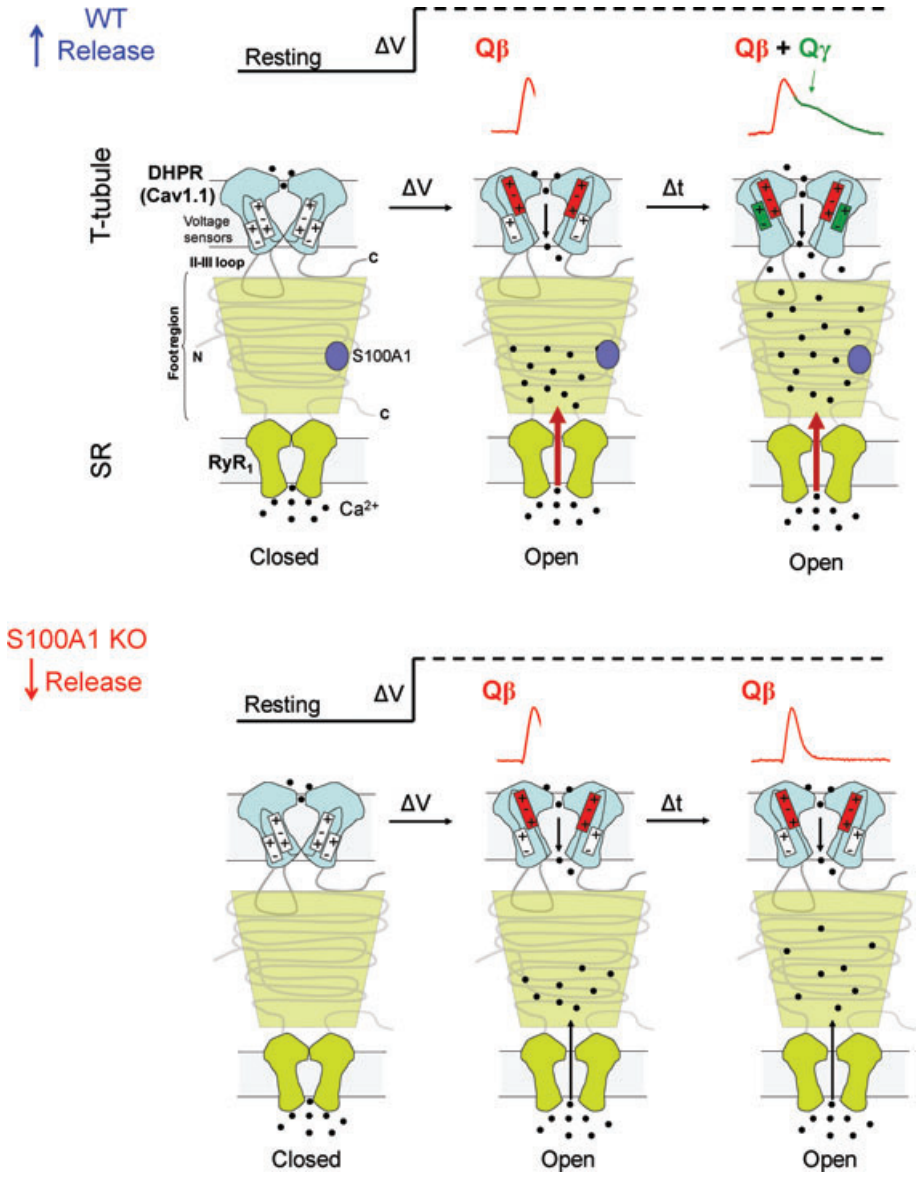

Figure 10. Model for the effects of Ca^{2+} release on charge movement in WT and S100A1 KO fibres
A, proposed effects of Ca^{2+} release on charge movement in WT fibres. Upon depolarization, charged residues in the α_1s subunit of the DHPR (cylinders in DHPR cartoon) act as voltage sensors that transduce its movement (Q_β) through the II–III loop into conformational changes that are sensed by the RyR1 and initiate Ca^{2+} release (middle cartoon). In WT fibres, S100A1 binding to the cytoplasmic foot of RyR1 enhances channel open time and optimizes release. This optimized Ca^{2+} release results in an elevation of local Ca^{2+} in the vicinity of a putative Ca^{2+} binding site regulating the generation of Q_γ by the DHPR (right cartoon). *B*, proposed effects of the absence of S100A1 on Ca^{2+} release and charge movement. In this scenario, the lower rate of Ca^{2+} release (middle cartoon) and the subsequently blunted local Ca^{2+} gradient, due to the lack of S100A1, simply does not reach the 'optimal' level required for the Ca^{2+}-dependent step(s) needed for the generation of Q_γ (right cartoon). Q_γ may arise from the further movement of the same set of voltage sensors that generate Q_β, or from a parallel set of charges uncoupled to the activation pathway. The function of this additional component of charge movement remains to be determined.

fibres compared to fibres from WT littermates, the time course of the release waveform was essentially unaltered. Furthermore, the voltage dependence of Ca^{2+} release was the same, except for a scaling factor, in fibres from WT and KO fibres. In this case, movement of some Q_β in WT fibres during depolarization (Fig. 10, top centre) would activate sufficient SR Ca^{2+} release to generate Q_γ, presumably by released Ca^{2+} interacting with the voltage sensor and thereby causing an additional component of charge movement (Fig. 10, right), as suggested earlier for frog fibres (Pizarro *et al.* 1991). Then the absence of Q_γ in fibres from KO mice is simply explained by the lower rate of release observed at all voltages in KO fibres (Fig. 10, bottom). The lower rate of Ca^{2+} release simply does not reach the level required for the Ca^{2+}-dependent step(s) needed for the appearance of Q_γ in the KO fibres. Consistent with the link between release amplitude and appearance of Q_γ, atypical KO fibres that exhibit unusually high release rates (for the KO fibres) also exhibited definite Q_γ in their charge movement records. A straightforward effect of S100A1 on RyR channel gating that could account for these observations would be for the mean RyR channel open time to be longer in the presence of S100A1 then in its absence, as previously observed in bilayer studies (Treves *et al.* 1997). In this case, on average there would be a greater amount of Ca^{2+} released during each channel opening in WT compared to S100A1 KO fibres, and a consequent larger increase in local Ca^{2+} in the vicinity of a putative Ca^{2+} binding site regulating the generation of Q_γ by intra-membrane voltage sensors.

In contrast to the simple uniform increase in release at all voltages seen in WT compared to S100A1 KO fibres, the addition of 4-CMC to KO fibres caused a shift of release activation to lower depolarizations, but with little or no change in the maximum rate of Ca^{2+} release. This is likely to have reflected a change in the coupling efficiency between charge moved and channel activation, and caused Q_γ to appear for intermediate depolarizations, but not for the largest depolarizations where release was not altered.

The exact charged residues that contribute to Q_γ, as well as their function, remain undetermined. Q_γ may arise from the further movement of the same set of voltage sensors that generate Q_β, or from a parallel set of charges uncoupled to the activation pathway (Bezanilla, 2000). Recent work has demonstrated several non-conducting functions of voltage-gated ion channels, such as the activation of enzymatic pathways by α and β subunits of ion channels (reviewed in Kaczmarek, 2006). It is tempting to speculate that Q_γ may contribute to some alternative cell signalling pathway in skeletal muscle fibres.

Summary

In summary, here we demonstrate that Ca^{2+} release flux is suppressed, but unchanged in voltage dependence and relative time course, in FDB muscle fibres lacking S100A1. We also identify a clear correlation in both WT and S100A1 KO fibres between Ca^{2+} release flux and the presence of a temporally delayed component of intra-membrane charge movement, Q_γ. We propose that the decreased release flux in S100A1 KO fibres, presumably due to the removal of a direct modulator of RyR1, accounts for the suppression of the Ca^{2+}-activated Q_γ component in KO fibres. This is supported by the finding that 4-CMC potentiates release flux during depolarizations to intermediate voltages and consequently restores Q_γ in KO fibres. Thus Q_γ may serve as an indicator of optimized local Ca^{2+} release at the triad junction. These findings shed light on the nature of RyR1 modulation and further our understanding of the complex bi-directional signalling between RyR1 and the DHPR.

References

Bezanilla F (2000). The voltage sensor in voltage-dependent ion channels. *Physiol Rev* **80**, 555–592.

Csernoch L, Pizarro G, Uribe I, Rodríguez M & Ríos E (1991). Interfering with calcium release suppresses I_γ, the 'hump' component of intramembranous charge movement in skeletal muscle. *J Gen Physiol* **97**, 845–884.

Delbono O & Stefani E (1993). Calcium transients in single mammalian skeletal muscle fibres. *J Physiol* **463**, 689–707

Fano G, Marsili V, Angelella P, Aisa MC, Giambanco I & Donato R (1989) S100a0 protein stimulates Ca^{2+}-induced Ca^{2+} release from isolated sarcoplasmic reticulum vesicles. *FEBS Lett* **255**, 381–384.

García J, Pizarro G, Ríos E & Stefani E (1991). Effect of the calcium buffer EGTA on the 'hump' component of charge movement in skeletal muscle. *J Gen Physiol* **97**, 885–896.

Gonzalez A & Rios E (1993). Perchlorate enhances transmission in skeletal muscle excitation-contraction coupling. *J Gen Physiol* **102**, 373–421.

Hui CS (1983). Differential properties of two charge components in frog skeletal muscle. *J Physiol* **337**, 531–552.

Huang CL (1988). Intramembrane charge movements in skeletal muscle. *Physiol Rev* **68**, 1197–1147.

Harkins AB, Kurebayashi N & Baylor SM (1993). Resting myoplasmic free calcium in frog skeletal muscle fibres estimated with fluo-3. *Biophys J* **65**, 561–562.

Hinkle PM, Shanshala ED & Nelso EJ (1992). Measurement of intracellular cadmium with fluorescent dyes. *J Biol Chem* **287**, 25553–25559.

Herrmann-Frank A, Richter M, Sarközi S, Mohr U & Lehmann-Horn F (1996). 4-Chloro-m-cresol, a potent and specific activator of the skeletal muscle ryanodine receptor. *Biochim Biophys Acta* **1289**, 31–40.

Jiménez-Moreno R, Wang ZM, Gerring RC & Delbono O (2008). Sarcoplasmic reticulum Ca^{2+} release declines in muscle fibres from aging mice. *Biophys J* **94**, 3178–3188.

Kaczmarek L (2006). Non-conducting functions of voltage-gated ion channels. *Nat Rev Neurosci* **7**, 761–771

Klein MG, Simon BJ, Szucs G & Schneider MF (1988). Simultaneous recording of calcium transients in skeletal muscle using high- and low-affinity calcium indicators. *Biophys J* **53**, 971–988

Klein MG, Lacampagne A & Schneider MF (1997). Voltage dependence of the pattern and frequency of discrete Ca^{2+} release events after brief repriming in frog skeletal muscle. *Proc Natl Acad Sci U S A* **94**, 11061–11066.

Liu Y, Carroll SL, Klein MG & Schneider MF (1997). Calcium transients and calcium homeostasis in adult mouse fast-twitch skeletal muscle fibres in culture. *Am J Physiol Cell Physiol* **272**, C1919–1927.

Melzer W, Rios E & Schneider MF (1984). Time course of calcium release and removal in skeletal muscle fibres. *Biophys J* **45**, 637–641.

Most P, Remppis A, Weber C, Bernotat J, Ehlermann P, Pleger ST, Kirsch W, Weber M, Uttenweiler D, Smith GL, Katus HA & Fink RH (2003). The C terminus (amino acids 75–94) and the linker region (amino acids 42–54) of the Ca^{2+}-binding protein S100A1 differentially enhance sarcoplasmic Ca^{2+} release in murine skinned skeletal muscle fibres. *J Biol Chem* **278**, 26356–26364.

Melzer W, Schneider MF, Simon BJ & Szucs G (1986). Intramembrane charge movement and calcium release in frog skeletal muscle. *J Physiol* **373**, 481–511.

Pizarro G, Csernoch L, Uribe I, Rodríguez M & Ríos E (1991). The relationship between Q_γ and Ca release from the sarcoplasmic reticulum in skeletal muscle. *J Gen Physiol* **97**, 913–947.

Prosser B, Wright N, Hernandez-Ochoa E, Varney K, Liu Y, Olojo R, Zimmer D, Weber D & Schneider M (2007). S100A1 binds to the calmodulin-binding site of ryanodine receptor and modulates skeletal muscle excitation-contraction coupling. *J Biol Chem* **283**, 5046–5057.

Prosser B, Hernandez-Ochoa E, Zimmer D & Schneider M (2009). The Q_γ component of intra-membrane charge movement is present in mammalian muscle fibres, but suppressed in the absence of S100A1. *J Physiol* **587**, 4523–4541.

Royer L, Pouvreau S & Ríos E (2008). Evolution and modulation of intracellular calcium release during long-lasting, depleting depolarization in mouse muscle. *J Physiol* **586**, 4609–4629.

Ríos E & Pizarro G (1991). Voltage sensor of excitation-contraction coupling in skeletal muscle. *Physiol Rev* **71**, 849–908.

Schaefer T, Beters J & Beyersmann D (1994). Cadmium uptake and interference with receptor-mediated calcium mobilization in PC12 cells. *Metal Ions in Biology and Medicine*, 149–154.

Schneider MF & Simon BJ (1988). Inactivation of calcium release from the sarcoplasmic reticulum in frog skeletal muscle. *J Physiol* **405**, 727–745.

Shirokova N, García J, Pizarro G & Ríos E (1996). Ca^{2+} release from the sarcoplasmic reticulum compared in amphibian and mammalian skeletal muscle. *J Gen Physiol* **107**, 1–18.

Shibuya I & Douglas WW (1992). Calcium channels in rat melanotrophs are permeable to manganese, cobalt, cadmium, and lanthanum, but not to nickel: evidence provided by fluorescence changes in fura-2-loaded cells. *Endocrinology* **131**, 1936–1941.

Simon BJ, Klein MG & Schneider MF (1991). Calcium dependence of inactivation of calcium release from the sarcoplasmic reticulum in skeletal muscle fibres. *J Gen Physiol* **97**, 437–471.

Simon BJ & Hill DA (1992). Charge movement and SR calcium release in frog skeletal muscle can be related by a Hodgkin-Huxley model with four gating particles. *Biophys J* **61**, 1109–1116.

Struk A & Melzer W (1999). Modification of excitation-contraction coupling by 4-chloro-m-cresol in voltage-clamped cut muscle fibres of the frog. *J Physiol* **515**, 221–231.

Treves S, Scutari E, Robert M, Groh S, Ottolia M, Prestipino G, Ronjat M & Zorzato F (1997). Interaction of S100A1 with the Ca^{2+} release channel (ryanodine receptor) of skeletal muscle. *Biochemistry* **36**, 11496–11503.

Wang ZM, Messi ML & Delbono O (1999). Patch-clamp recording of charge movement, Ca^{2+} current, and Ca^{2+} transients in adult skeletal muscle fibres. *Biophys J* **77**, 2709–2716.

Westerblad H, Andrade FH & Islam MS (1998). Effects of ryanodine receptor agonist 4-chloro-m-cresol on myoplasmic free Ca^{2+} concentration and force of contraction in mouse skeletal muscle. *Cell Calcium* **24**, 105–115.

Zorzato F, Scutari E, Tegazzin V, Clementi E & Treves S (1993). Chlorocresol: an activator of ryanodine receptor-mediated Ca^{2+} release. *Mol Pharmacol* **44**, 1192–201.

Author contributions

B.L.P. performed the experimentation, analysis, and writing involved with this work. E.O.H. contributed to experimental design, interpretation of results, and drafting of the manuscript. D.B.Z. designed and provided the S100A1$^{-/-}$ animal and WT counterparts, and also critically revised and approved the final manuscript. M.F.S contributed to experimental design, analysis, interpretation, discussion and drafting of the manuscript. All the experiments presented above were performed in the laboratory of M.F.S., University of Maryland, Baltimore.

Acknowledgements

The project described was supported by grant number RO1 AR055099 from the National Institute of Arthritis and Musculoskeletal and Skin Diseases, NIH. B.L.P. was supported by NIAMS training grant T32 AR007592 to the Interdisciplinary Program in Muscle Biology, University of Maryland School of Medicine.